International Journal of Bioelectromagnetism
IJBEM

Volume 3, Number 2, pp. 49-58, 2001.

Segmentation of MR Images using Deformable Models: Application to Cardiac Images

Jyrki MP Lötjönen

VTT Information Technology, Tampere, Finland
Laboratory of Biomedical Engineering, Helsinki University of Technology, Finland

Correspondence: J Lötjönen, Human Interaction Technologies, VTT Information Technology, P.O. Box 1206, FIN-33101 Tampere, Finland. E-mail: jyrki.lotjonen@vtt.fi, phone +358 3 316 3378, fax +358 3 317 4102

Abstract. This paper discusses various aspects related to the segmentation of cardiovascular magnetic resonance images using deformable models. A short survey on segmentation techniques is first presented. Thereafter, a recently developed method, based on a volumetric template, is demonstrated in two case studies. The method is applied to the segmentation of the heart, and to the motion tracking of the heart. In the both cases, the method produced overall good results with minor errors.

Keywords: Cardiovascular Segmentation; Model-based Segmentation; Elastic Matching; Motion Tracking; MR Imaging.

1. Introduction

Segmentation is often a pre-requisite for many applications utilizing medical images, such as for making dose planning in radiotherapy, and for visualizing three-dimensional (3D) data in surgical planning. Since modern medical imaging systems can generate even hundreds of slice images from an object of interest, the extraction of shape knowledge by manual segmentation is a long and tedious process. Therefore, a great number of different approaches, such as region growing, fuzzy clustering and neural networks, has been proposed to automate the segmentation process [Acharya and Menon, 1998]. However, a generally applicable, fast, fully automated and robust method for segmenting human organs is still not available. The segmentation of medical images can be particularly challenging even for a specialist because the images contain typically complex noisy structures and may also lack some anatomical borders. The use of *a priori* knowledge is, therefore, often essential. In the techniques referred to as deformable models, *a priori* knowledge is incorporated by making assumptions on the final segmentation result; the result can be constrained to be, for example, a smooth continuous surface. The methods based on deformable models are widely used in medical image segmentation and motion tracking [McInerney and Terzopoulos, 1996]. The optimal method for a given problem depends highly on the characteristics of the application; the models themselves as well as the techniques to deform them vary appreciably.

This paper concentrates on cardiovascular segmentation and motion tracking using magnetic resonance (MR) images. However, the methods discussed are generally applicable for many other application areas and imaging modalities. In the next section, a short survey is

presented on deformable models, emphasizing the aspects related to cardiovascular images. Thereafter, one recently proposed technique [Lötjönen et al., 2001] is discussed in detail and applied in two case studies: 1) the segmentation of a short-axis cardiac MR volume and 2) the motion tracking of the heart using a short-axis cine MR volume. Finally, the discussion is presented.

2. Related Work

2.1. Models Preserving the Topology without a Priori Shape Knowledge

The most well known deformable model is a physics-based active contour model, also referred to as a snake [Kass et al., 1987]. The position of the snake is described by a parametric function: $\mathbf{v}(s)=(x(s),y(s))$, $s\hat{I}\ [0,1]$. It is deformed by minimizing energy consisting of physics-based internal and external constraint forces, and forces derived from the image to be segmented:

$$E(v) = \int_0^1 (\omega_1(s)\left|\frac{\partial \mathbf{v}}{\partial s}\right| + \omega_2(s)\left|\frac{\partial^2 \mathbf{v}}{\partial s^2}\right|)ds + \int_0^1 P(\mathbf{v}(s))\,ds + \int_0^1 E_{ext}\,ds, \qquad (1)$$

where the first integral depicts the internal energy of the snake due to stretching and bending respectively. The functions $w_1(s)$ and $w_2(s)$ give a balance between the physical properties of the model as well as between the physical properties and the other forces. The scalar field $P(v)$ represent image forces, which are usually defined from image features, such as the local image intensity or gradient. The external constraints are included in the last integral, e.g. a user specified repulsion force at a fixed position. The energy minimum is found numerically by solving the Euler-Lagrange equation.

If the initialization of the snake is far from the desired result, the model may deform to an incorrect local minimum; initialization is a well-known problem related to deformable models. In the original article, the robustness was improved by using the *scale-base* approach, where the image is low-pass filtered before computing the image forces represented by gradients. Low-pass filtering leads to noise reduction and increases the attraction range to salient edges. In the widely adopted *multi-resolution* approach [Bajcsy and Kovacic, 1989], the images were low-pass filtered and subsampled sequentially. The modeling is done first for the lowest resolution data and the result is used as an initialization for the next higher resolution data. In addition to the advantages from the scale-base approach, the computational complexity of the deformation is then reduced. The attraction field can be extended even more by a distance transformation computed for binarized images [Borgefors, 1986], but the problem is often to find a good binarization. More degrees of freedom, often at higher frequencies, are gradually added to the deformation in the *global-to-local approach*, i.e. a global alignment is defined before local matching. In addition to these standard techniques, many other improvements have been reported, such as using a balloon force inflating or deflating the model across local minima [Cohen, 1991], and applying dynamic programming to find the global energy minimum [Geiger et al., 1995].

Conventional snake-based methods appear to be well suited to shape reconstruction, but they do not fit well to object recognition. The aim of the object recognition is to describe the deformations with relatively few parameters. Therefore, methods such as standard engineering technique *finite element methods (FEM)* technique have been used to parameterize the deformations. A parameterization can be obtained from the eigenvectors of the FEM model corresponding to the object [Pentland and Horowitz, 1991]. Another method is to combine global and local representations. Superquadrics can be used to describe the global shape of the object, whereas the object is locally deformed using the FEM basis functions [Gupta et al., 1994]. Alike method, without using the physics-based approach and the FEM, combines superquadrics and free-form deformations (FFD) [Bardinet et al., 1998]. In the FFD, a model is positioned inside of a regular grid and the model is deformed according to the grid point displacements using linear or spline interpolation.

Highly convoluted objects, such as the human cortical surface, are frequently segmented from MR images using hybrid methods by applying sequentially several image processing operations [Dale et al., 1999; Xu et al., 1999]. The initial surface or a pre-segmentation is usually extracted by using different image processing techniques, such as local intensity-based segmentation methods and morphological operations. The final surface is generated using deformable models.

2.2. Models Preserving the Topology with a Priori Shape Knowledge

A priori shape knowledge, depicted often by a template, represents the typical shape of the object to be reconstructed. If a shape template is provided, the initialization problem of the conventional snake-based methods is, at least partly, overcome and the segmentation process becomes more robust.

In probabilistic deformable models, the shape of the object was represented by a weighted sum of orthogonal functions, such as Fourier basis-functions, where the probability distributions for the weights, i.e. the parameters, were known [Staib and Duncan, 1996]. The distributions were determined from a training set. The mean of the distributions defined the initial model, and the deformation followed the deviation of the distribution around the mean. An objective function to be maximized during the deformation was the sum of two terms indicating the probability of the parameters and the degree of correspondence between the model and the image. In probabilistic models, the ability to represent different topologies is limited and a high number of harmonics are needed to model highly convoluted objects.

The Active shape model (ASM), proposed by [Cootes et al., 1995], defines the mean model and its deformation modes consistent with a training set by statistical computations. The model consists of a point set. The mean model is computed by defining the point-to-point correspondence between the different models in the training set, and by calculating an average for the points. A covariance matrix is computed for the displacements from the mean model. The eigenvectors of the covariance matrix define the deformation modes of the mean model. The deformation is accomplished iteratively by defining the magnitudes for the deformation modes, which move the model toward the strongest image edges. Instead of using the ASM, the model can be represented by Fourier basis-functions and the deformation modes of the training set can be defined by performing the principal component analysis to the Fourier coefficients [Székely et al., 1996]. A major problem of statistical models is that the building of a representative training set can be laborious, if the point-to-point correspondence definition cannot be automated. Active appearance model (AAM) extends ASM by modeling also the gray-scale variability [Cootes, 1999]. In the final matching result, both the shape and the appearance of the model should match the destination data. In [Mitchell et al., 2001], the ASM and AAM were combined into a hybrid model.

Boundary template models, represented by a contour(s) in 2D or a surface(s) in 3D, are similar to statistical shape models, except that the model is not necessary a mean in statistical sense, and it is not deformed using statistically defined modes. The boundary templates can be deformed using methods similar to the snakes considering, for example, material stiffness and bending; the difference is that the initialization is pre-defined. The template used in [Lelieveldt et al., 1999] was a geometric and topologic model representing thorax, lungs, epicardium, ventricles and liver. The organs were modeled using multiple hyperquadric surfaces. The model was matched to the boundaries in the image by varying the scale and the pose of the hyperquadrics. A set of triangulated surfaces was matched to noisy binarized edges using FFD in [Lötjönen et al., 1999]. The change in the model's shape was regulated during the deformation. In addition, the multi-resolution and the global-to-local approaches were used.

A volumetric template is an extension of the boundary templates. The volumetric template is a volume data set, where each voxel contains a vector consisting of real and symbolic information, such as an anatomic label and gray-scale information from an MR volume. If tissue classes are included in the template, it is referred to as an atlas. Volumetric templates can be constructed by segmenting, possibly manually, the organs of interest from a

representative data volume. The volumetric templates are matched with the patient data by maximizing a correlation measure. In [Christensen et al., 1996], physical properties of either elastic solids or fluids were simulated in the deformation. The difference between the gray values of the model and data were minimized while keeping simultaneously the transformation smooth. The transformation was also constrained to be smooth in [Rueckert et al., 1999] but mutual information (MI) was used as a similarity measure. The model was deformed using FFD.

2.3. Models Allowing Changes in the Topology

In general, the major problem in the snake-based methods is that the model should be initialized reasonably close to the desired shape. Moreover, the snake-based methods do not easily recover shapes containing high frequency components, such as protrusions. A level-set approach was designed to overcome these problems [Malladi et al., 1995]. The method is based on the idea of propagating wave fronts with curvature-dependent speeds. The method is relatively independent on the initialization and can produce protrusions, such as in a human vessel trees, and changes in topology of the model. Alternatively, a method based on a dynamic triangulated model using Newtonian dynamics, and adapting its topology and geometry according to input data can be applied [Lachaud et al., 1999]. The deformation is controlled by internal constraints, such as the surface curvature and the distance between the nodes in the triangulation, and external constraints, such as forces defined by the intensities of the input data. In [McInerney and Terzopoulos, 1999], the formulation of the snakes was extended producing T-snakes. T-snake is a normal snake, which is projected on a regular grid and thereafter reparameterized during each iteration step. Reparameterization allows changes in the topology.

2.4. Aspects Related to Cardiovascular Segmentation

Segmentation of heart. Several of the reviewed papers, such as [Bardinet et al., 1998; Cohen, 1991; Geiger et al., 1995; Gupta et al., 1994; Lelieveldt et al., 1999; Lötjönen et al., 1999; Mitchell et al., 2001; Staib and Duncan, 1996], were applied to the segmentation of the heart, i.e. the left ventricle (LV), the right ventricle (RV) and/or the epicardium The segmentation of the epicardium is problematic. In some regions, there are no visible edges between the myocardium and surrounding tissues. For this reason, deformable models, especially template-based methods, are needed to estimate the lacking edges. The other problem is that some people have, in practice, no fat around epicardium while some people may have several millimeters. If the fat is present, the model attaches easily to the strongest edge between the lungs and the epicardium. The techniques modeling appearance can cope the problem. The segmentation of the ventricles is more straightforward, but still the noise and imaging artifacts may cause problems. In addition, doctors use to segment the ventricles by drawing a convex hull surrounding blood masses. The most of the deformable models attach, however, to the strongest edges and follow the papillary muscles inside the convex hull. The problem can be solved by volumetric transformations as the desired hull is transformed after the segmentation using the defined transformation.

Segmentation of vessels. The segmentation of the vessel trees was demonstrated in [Malladi et al., 1996; McInerney and Terzopoulos, 2001]. The template-based methods cannot solve the problem, because of high variability between humans. In addition, conventional snakes cannot recover protrusion very well, but interactive software packages utilizing snakes exist [Liang, 2001].

Motion tracking. In MR imaging, the dynamic behavior of the organs can be modeled using cine sequences, i.e. several images are acquired from the same location at different time instants. Motion tracking of the heart was demonstrated in [Pentland and Horowitz, 1991; Nastar and Ayache, 1996]. The methods based on volumetric templates produce motion vectors for the whole image area without segmentation. However, motion tracking of a specific organ and its quantification is usually required. In that case, data from one time instant need to be segmented, and it is used as a model for the motion tracking. If segmentation is available for all time instants, methods utilizing surface metrics can be used,

e.g. matching surface areas with similar curvatures [Kambhamettu and Goldgof, 1994]. Parametric models or deformations are the most feasible, if the quantification of the motion is desired. The strength of the parametric methods is that the motion is characterized using a small set of parameters. Finally, it is worth noting that the deformation to the closest edge point, as often used in deformable models, does not necessarily represent the real motion of an organ. For example, the twisting of the heart is difficult to model with conventional methods. The MR technique referred to as tagging is used to model the exact motion.

3. Material and Methods

Next, one method [Lötjönen and Mäkelä, 2001] is presented in detail.

3.1. Matching Using a Volumic Template

The model used is a volumetric template consisting of two components: a gray-scale volume and triangulated surfaces of the objects of interest. In this study, the volume of the size 128x128x125 is a T1 weighted short-axis MR volume of the heart (Fig. 1). The surfaces included in the model are the epicardium, the LV and the RV.

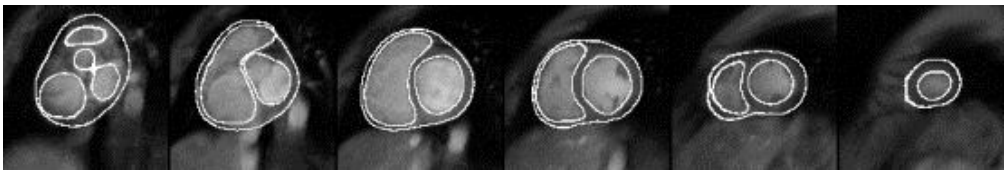

Figure 1. Volumetric template: a set of slices from the gray-scale volume and the triangulated surfaces superimposed on the images.

The model needs to be rigidly registered, i.e. translated and rotated, to a destination data volume before elastic matching. In practice, the translation errors of a few voxels and the rotation errors of several degrees are acceptable. Automated methods exist but manual coarse registration can be done in a couple of minutes.

In the following, the model volume is referred to as a *volume M*, and the destination volume to which the model is matched, *volume D*. Consequently, a voxel from the volumes *M* and *D* are $\mathbf{m}=(m_1,m_2,m_3)$ and $\mathbf{d}=(d_1,d_2,d_3)$, respectively.

The elastic transformation function is determined by maximizing a similarity function between the model and data. The similarity function consists of three components: MI, joint gradient information and shape regularization.

Mutual information. MI measures the degree of dependence between the volumes *M* and *D*. MI is high if the gray-scale value of a voxel in *D* can be estimated with a high accuracy by knowing the gray-scale value of the corresponding voxel in *M*. The similarity criterion based on MI allows matching also images from different imaging modalities. As the gray-scale values of the volumes *M* and *D* are considered random variables *A* and *B*, respectively, MI is computed from the equation [Maes et al., 1998] :

$$E_{MI} = \sum_{a,b} p_{AB}(a,b) \log \frac{p_{AB}(a,b)}{p_A(a)\,p_B(b)}, \qquad (2)$$

where $p_A(a)$ and $p_B(b)$are marginal probabilities and $p_{AB}(a,b)$ is the joint probability distribution. $p_A(a)$ is a probability that the gray-scale value of a voxel in *M* is *a*. $p_{AB}(a,b)$ is a probability that the gray-scale values of corresponding voxels in *M* and *D* are *a* and *b*, respectively.

Joint gradient information. The edges in *M* should match similarly oriented edges in *D*. The similarity criterion derived from the image gradients is computed as follows [Pluim et al., 2000]:

$$E_{grad} = \frac{1}{N} \sum_{(\mathbf{m},\mathbf{d}) \in (M \cap D)} \frac{\nabla \mathbf{m} \cdot \nabla \mathbf{d}}{|\nabla \mathbf{m}||\nabla \mathbf{d}|} \min(|\nabla \mathbf{m}|, |\nabla \mathbf{d}|), \quad (3)$$

where *N* is the number of model points overlapping the volume *D*. The intensity ranges of the volumes *M* and *D* should be set nearly similar before the matching. If inter-modality matching is used, the equation is modified by taking an absolute value from the dot-product.

Shape regularization. The change in the shape of the model surfaces is constrained during the matching. In this study, the change of the model's surface normals is controlled. The shape similarity of the original model and the deformed model is computed as follows:

$$E_{model} = \frac{1}{N_{tr}} \sum_{i=1}^{N_{tr}} \mathbf{n}_i \cdot \mathbf{n}_i^0, \quad (4)$$

where N_{tr} is the total number of triangles in the model surfaces, $\mathbf{n_i}$ and $\mathbf{n_i^0}$ are the deformed and the original orientations of the surface normals of the triangles, respectively.

Combined similarity criterion. The model is deformed by maximizing the following total similarity criterion:

$$E_{total} = E_{MI} + \alpha E_{grad} + \beta E_{model}, \quad (5)$$

where a and b are user-specified weight parameters for different similarity components.

The transformation is applied to all model points, i.e. the voxels and surface points, which are inside the region defined by a deformation sphere. The sphere is positioned into a high number of locations (>10000) and the transformation is applied sequentially in each position. The center of the sphere is randomly positioned on the surfaces of the model.

Fig. 2 demonstrates the functionality of the deformation sphere, which is shown by the big circle containing arrows. The dark and light gray areas on the left represents a part of the myocardium and the left ventricle, respectively. The arrows (vectors) in Fig. 2 describe the displacements for the model points in the corresponding positions. A displacement vectors are derived from the vector posed to the center of the sphere (bold arrow in the center). The vector in the center is weighted by a Gaussian kernel in such a way that the weight is one in the center and zero on the sphere surface and outside of it. The purpose of the deformation algorithm is to find an optimal displacement by determining a vector for the center. In practice, several different vectors are tested (usually 6-12 vectors in 3D), the corresponding displacement fields are applied to the model, and the one producing the highest similarity value (Eq. 5) is chosen. The orientation of each tested vector is randomly chosen. The small circle with light center and dark borders visualizes the probability distribution for different vector orientations and lengths: the lighter is the gray-value the higher is the probability. The probability distribution is a Gaussian function preferring small displacements. The displacements outside the small circle are prohibited.

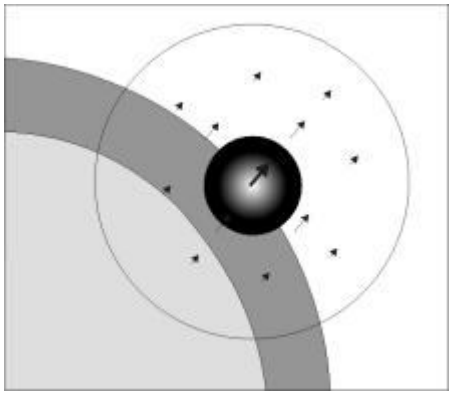

Figure 2. Displacement vectors inside a deformation sphere.

The global-to-local approach is used in the method. This is accomplished by decreasing gradually the size of the deformation sphere during iterations. The user specifies the maximum and the minimum radius for the sphere. The size is reduced as the value of the similarity function does not decrease more than e during an iteration. The number of spheres applied for one iteration is relative to the volume of the model divided by the volume of the sphere.

The multi-resolution approach is also adopted, i.e. a low resolution model volume is produced by Gaussian filtering and subsampling a high resolution volume. The deformation is first done for the lowest resolution volume. As the maximum similarity value is attained, the transformation defined is applied as an initialization for the higher resolution level.

3.2. Image Data

Segmentation. The destination data used was a T1-weighted short-axis MR data volume from the heart (Siemens Magnetom Vision 1.5 T system at the Department of Radiology in Helsinki University Central Hospital, Finland). The original volume consisted of 18 slices of 256x256 pixels. The pixel size was 1.36 mm x 1.36 mm and the slice thickness 10.0. However, the data volume was interpolated to isotropic and only the area containing the heart was extracted from the original volume for the segmentation. The final volume segmented was the size of 128x128x125 voxels.

Motion tracking. The data used in motion tracking were similar to the data used in segmentation except the data contained 10 volumes from various time instances during the cardiac cycle. The time difference between the volumes was 40 ms.

4. Results

4.1. Segmentation of the Heart

Fig. 3 shows a set of slices from the destination data and the model superimposed on the data before (the top row) and after (the bottom row) the deformation. The overall result is good. However, we have also developed an interactive 3D software package by which the possible segmentation errors can be corrected in a few seconds.

Four resolution levels were used in matching. The user-defined parameters in Eq. 5 were a=2 and b=15. The size of the deformation sphere varied from 15 to 5 at each resolution level. The computation time using a standard PC (600 MHz Pentium) was a few minutes.

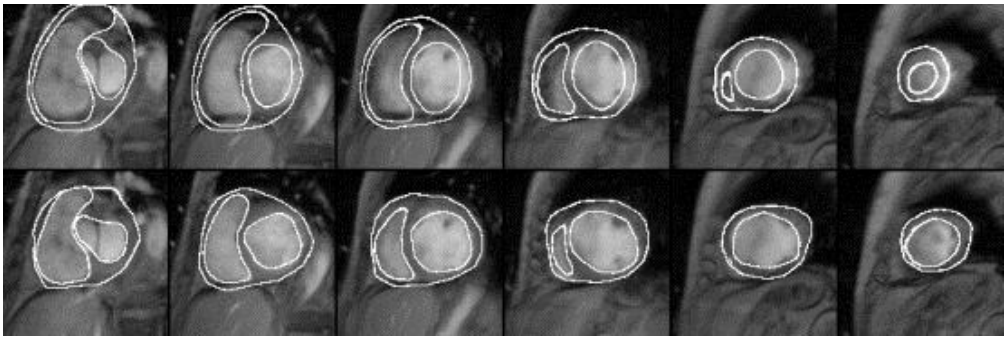

Figure 3. Segmentation of the epicardium, LV and RV. Upper row: The model surfaces superimposed on the destination data before (the top row) and after (the bottom row) matching.

4.2. Motion Tracking of the Heart

The four rows of Fig. 4. show a set of slices from end-diastolic phase to systolic phase. Each image visualizes gray-scale values from two volumes using the chessboard visualization technique. The first row shows the original volume (t=2) with the result as the volume (t=1) is matched to the volume (t=2). The second, third and fourth rows visualize the original volumes (t=3, t=4 and t=5), respectively, with the deformed data as the result from the previous time instant (t=2, t=3 and t=4) is used as an initial model. In other words, the volume (t=1) is sequentially matched to the time instants from t=2 to t=5. The continuous edges of Fig. 4 show that the matching was able recover the motion reasonably well. Since the appearance is not modeled, the gray-scale differences between the volumes remain in the result, and the chessboard effect is visible.

Two resolution levels were used and the parameters in Eq. 5 were a=2 and b=10. The size of the deformation sphere varied from 15 to 6 at each resolution level.

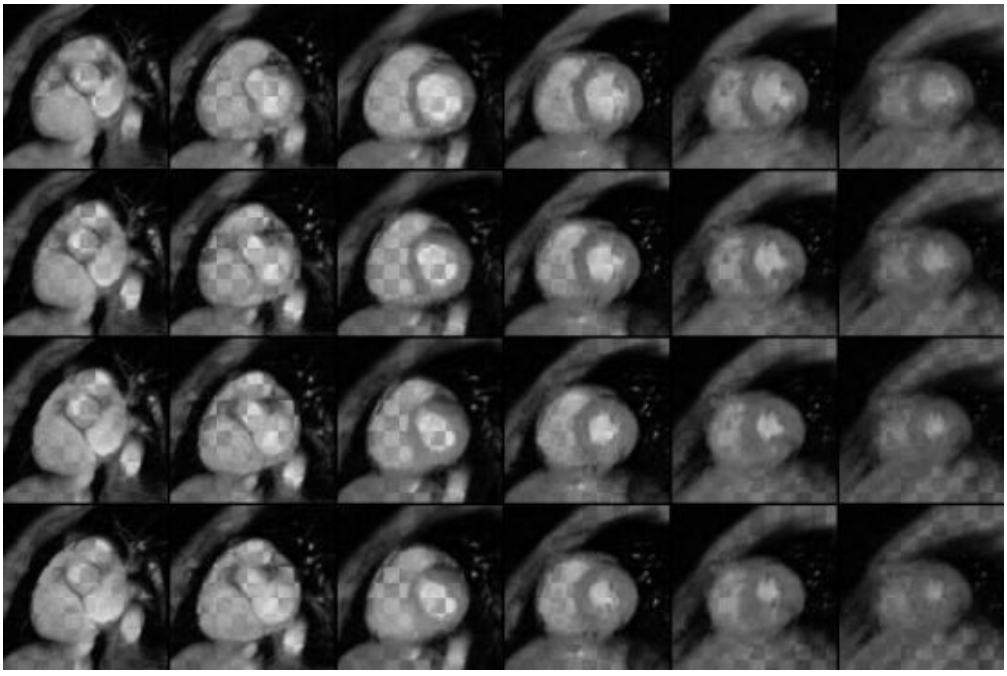

Figure 4. The rows from the top down visualize the volumes from time instants (t = 2, t = 3, t = 4 and t = 5). Chess-board visualization technique is used to show in each image gray-scale values from the original and deformed volumes, i.e.the areas shown from the deformed model and from the original data vary as the black and white areas in the chessboard. The volume (t = 1) is used as a model.

5. Discussion

Deformable models are widely used in medical image segmentation. In general, deformable models are superior to the techniques utilizing local intensity criteria, if edges in the data to be segmented are unclear, e.g. noisy or incomplete. For example, the automatic segmentation of epicardium from MR images is extremely difficult without a priori knowledge, because images contain no clear edges in some regions between epicardium and surrounding tissues. Since deformable model techniques differ appreciably with each other, the feasibility of a specific technique for a given segmentation problem needs to be carefully considered.

A major problem of deformable models is to find an initial model, which is not too far from the desired edges. Even though the model was well-initialized, complex human structures, noise, imaging artifacts and imaging features, e.g. the ability to separate myocardium from surrounding tissues, can make the segmentation task difficult. In practice, a user-interaction is still needed in many cases.

The method, which was demonstrated in this work, estimated relatively well the epicardium as well as the LV and the RV. However, if the destination data contains fat around epicardium and the model not, the method fails to segment correctly the epicardium. Further development is needed to include the AAM like features to the method. The result of motion tracking appeared also visually good. The real motion of separate model points was not, however, known and the transformation defined could not be therefore validated. The tagging technique should be used to validate the result.

This work concentrated on MR images but cardiovascular hemodynamics could be studied using also other imaging modalities, such as X-ray imaging, computerized tomography, ultrasound imaging single photon emission tomography (SPET) and positron emission tomography (PET). The deformable model techniques described could be applied as well to these modalities but the segmentation of functional SPET and PET images is still a difficult problem even with deformable models.

Acknowledgements

The authors express thanks to The Department of Radiology, Helsinki University Central Hospital, Finland for providing volume images. Research work was supported by the National Technology Agency, Finland.

References

Acharya R, Menon RP. Review of biomedical image segmentation techniques, in Deformable models in medical image analysis. IEEE Computer Society Press, 140-161, 1998

Bajcsy R, Kovacic S. Multiresolution elastic matching. *Comp. Vis., Graph.. and Image Proc.*, 46: 1-21, 1989.

Bardinet E, Cohen LD, Ayache N. A parametric deformable model to fit unstructured 3d data. *CVGIP: Comp. Vis. and Image Understanding*, 71(1): 39-54, 1998.

Borgefors G. Distance transformation in digital images. *Comp. Vis, Graph. and Image Proc.*, 48: 344-371, 1986.

Christensen GE, Miller MI, Vannier MW, Grenander U. Individualizing neuroanatomical atlases using a massively parallel computer. *IEEE Computer*, January, 1996.

Cohen LD. On active contour models and balloons. *CVGIP: Image Understanding*, 53(2): 211-218, 1991.

Cootes TF, Taylor CJ, Cooper DH, Graham J. Active shape models – their training and application. *Comp. Vis. and Image Understanding*, 61(1): 38-59, 1995.

Cootes TF. Statistical models of appearance for computer vision. http://www.isbe.man.ac.uk/~bim/Models/app_model.ps.gz, 1999.

Dale AM, Fischl B, Sereno MI. Cortical surface-based analysis I. Segmentation and surface reconstruction. *NeuroImage*, 9: 179-194, 1999.

Geiger D, Gupta A, Costa LA, Vlontzos J. Dynamic programming for detecting, tracking and matching deformable contours. *IEEE Trans. Pattern Anal. Machine Intell.*, 17(3): 294-302, 1995.

Gupta A, O'Donnell T, Singh A. Segmentation and tracking of cine cardiac mr and ct images using a 3-D deformable model. In proceedings IEEE Conf. Computers in Cardiology, 1994, 661-664.

Kass M, Witkin A, Terzopoulos D. Snakes: Active contour models. *Int. J. Comp. Vis.*, 1: 321-331, 1987.

Kambhamettu C, Goldgof DB. Curvature-Based Approach to Point Correspondence Recovery in Conformal Nonrigid Motion. *CVGIP: Image Understanding*, 60(1): 26-43, 1994.

Lachaud JO, Montanvert A. Deformable meshes with automated topology changes for coarse-to-fine three-dimensional surface extraction. *Med. Image Anal.*, 3(2): 187-207, 1999.

Lelieveldt BPF, van der Geest RJ, Ramze Rezaee M, Bosch JG, Reiber JHC. Anatomical model matching with fuzzy implicit surfaces for segmentation of thoracic volume scans. IEEE Trans. Med. Imag., 18(3): 218-230, 1999.

Liang J, McInerney T, Terzopoulos D. Interactive medical image segmentation with United snakes. In Lecture Notes in Computer Science 1679: Medical Image Computing and Computer-Assisted Intervention, MICCAI99, C. Taylor, A. Colchester, Editors, Spriner, 1999, 116-127.

Lötjönen J, Reissman PJ, Magnin IE, Katila T. Model extraction from magnetic resonance volume data using the deformable pyramid. *Med. Image Anal.*, 3(4): 387-406, 1999.

Lötjönen J, Mäkelä T. Elastic matching using a deformation sphere. Medical image computing and computer assisted intervention 2001. (in press)

Maes F, Collignon A, Vandermeulen D, Marchal G, Suetens P. Multimodality image registration by maximization of mutual information. *IEEE Trans. Med. Imag.*, 16(2): 187-198, 1997.

Malladi R, Sethian JA, Vemuri BC. Shape modeling with front propagation: A level set approach. *IEEE Trans. Pattern Anal. Machine Intell.*, 17(2): 158-175, 1995.

McInerney T, Terzopoulos D. Deformable models in medical image analysis: a survey. *Med. Image Anal.*, 1(2): 91-108, 1996.

Mitchell SC, Lelieveldt BPF, van der Geest RJ, Bosch HG, Reiber JHC, Sonka M. Multistage Hybrid active appearance model matching: Segmentation of left and right ventricles in cardiac MR images. *IEEE Trans. Med. Imag.*, 20(5): 415-423, 2001.

Nastar C, Ayache N. Frequency-based nonrigid motion analysis: Application to four dimensional medical images. *IEEE Trans. Pattern Anal. Mach. Intell*, 18(11): 1067-1079, 1996.

Pentland A, Horowitz B. Recovery of nonrigid motion and structure. *IEEE Trans. Pattern Anal. Machine Intell.*, 13(7): 730-742, 1991.

Pluim JPW, Maintz JBA, Viergever MA. Image registration by maximization of combined mutual information and gradient information. *IEEE Trans. Med. Imag.*, 19(8): 809-814, 2000.

Rueckert D, Sonoda LI, Hayes C, Hill DLG, Leach MO, Hawkes DJ. Nonrigid registration using free-form deformations: Application to breast MR images. *IEEE Trans. Med. Imag.*, 18(8) 712-721, 1999.

Staib LH, Duncan JS. Model-based deformable surface finding for medical images. *IEEE Trans. Med. Imag.*, 15(5): 720-731, 1996.

Szekély G, Kelemen A, Brechbühler, Gerig G. Segmentation of 2-d and 3-d objects from mri volume data using constrained elastic deformations of flexible fourier contour and surface models. *Med. Image Anal.*, 1(1): 19-34, 1996.

Xu C, Pham DL, Rettmann ME, Yu DN, Prince JL. Reconstruction of the human cerebral cortex from magnetic resonance images. *IEEE Trans. Med. Imag.*, 18(6): 467-480, 1999.